Development and Testing of a High-Precision Position and Attitude Measuring System for a Space Mechanism

Nikolay Khanenya, Gabriel Paciotti*, Eugenio Forzani* and Luc Blecha*

Abstract

This paper describes a high-precision optical metrology system – a unique ground test equipment which was designed and implemented for simultaneous precise contactless measurements of 6 degrees-of-freedom (3 translational + 3 rotational) of a space mechanism end-effector [1] in a thermally controlled ISO 5 clean environment.

The developed contactless method reconstructs both position and attitude of the specimen from three cross-sections measured by 2D distance sensors [2]. The cleanliness is preserved by the hermetic test chamber filled with high purity nitrogen. The specimen's temperature is controlled by the thermostat [7]. The developed method excludes errors caused by the thermal deformations and manufacturing inaccuracies of the test jig.

Tests and simulations show that the measurement accuracy of an object absolute position is of 20 micron in in-plane measurement (XY) and about 50 micron out of plane (Z). The typical absolute attitude is determined with an accuracy better than 3 arcmin in rotation around X and Y and better than 10 arcmin in Z. The metrology system is able to determine relative position and movement with an accuracy one order of magnitude lower than the absolute accuracy. Typical relative displacement measurement accuracies are better than 1 micron in X and Y and about 2 micron in Z. Finally, the relative rotation can be measured with accuracy better than 20 arcsec in any direction.

Introduction

The metrology system was developed by Almatech (Switzerland) within the framework of the Solar Orbiter project. The mission overall goal is to produce images of the Sun at an unprecedented resolution and perform closest ever in-situ measurements. The Slit Change Mechanism (SCM) is part of the SPICE (SPectral Imaging of the Coronal Environment) instrument which provides spectral imaging of the solar disk, corona and characterizes plasma properties of the Sun. The SCM itself was previously presented at the 42nd Aerospace Mechanisms Symposium [1]. The SCM prototype is shown in Figure 1, the metrology system is shown in Figure 2.

The SCM end effector shall move with a high accuracy and repeatability. These performances shall be verified by test during qualification campaign. No off-the-shelf measurement equipment could be found that fulfils all requirements such as geometrical limitations, measurement accuracy, cleanliness, specimen surface properties, gravity direction, test repeatability, temperature stability, and temperature range. During the early stage of the project, a wide range of measurement means were studied. All contact measurement devices were ruled out as the specimen surface is delicate and the displacement introduced by any mechanical contact would bias the measurement. Indeed, the SCM end effector is only supported by leaf spring elements with low stiffness and thus its position is very sensitive to any external forces. Laser 3D scanners (e.g., [3]) have insufficient accuracy. Confocal 3D microscopes (e.g., [4]) and digital holographic microscopes (e.g., [5]) have a too small observation distance and a small field of view, which makes them incompatible with the test setup. X-ray 3D scanners (e.g., [6]) cannot be combined with an environment control system. Therefore, a unique high-precision measurement system was

* Almatech, Lausanne, Switzerland

developed. It combines Keyence sensors [2] and Huber thermostat [7] with Almatech software and hardware.

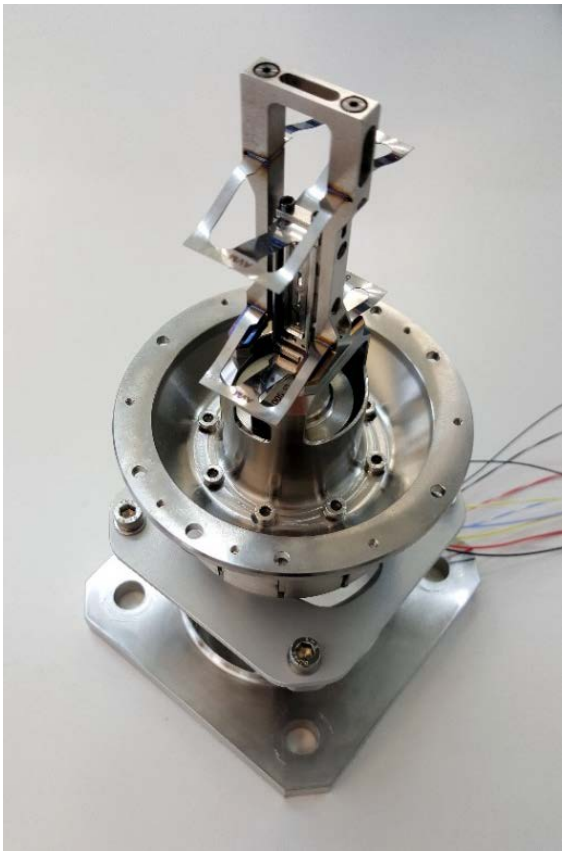

Figure 1. Slit Change Mechanism prototype

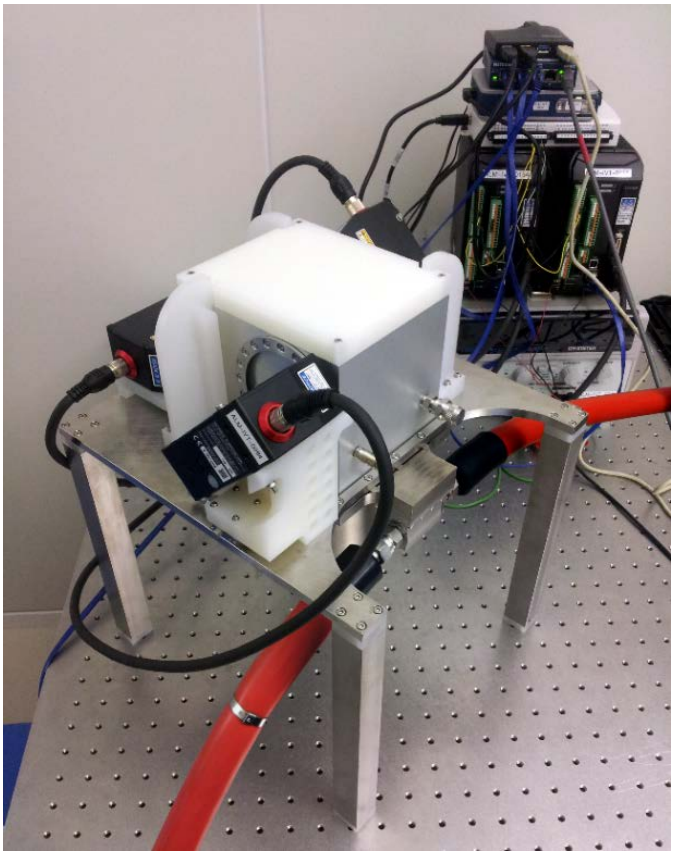

Figure 2. Metrology system

Key features

The metrology system has the following key features.

- **6 degrees-of-freedom**
  Simultaneous measurement of specimen's absolute position and attitude in 3D.
- **Clean environment**
  The environment around the specimen is clean and hermetically sealed.
  It is purged with high purity nitrogen, providing an environment better than ISO 5 (class 100).
- **Temperature control**
  Mechanical interface temperature is controlled by external thermostat [7] within the range from -40°C to +200°C with stability of 0.01°C. Change of the temperature does not affect spatial measurement accuracy as the measurement devices are thermally isolated from the observed specimen.
- **Contactless measurement**
  The measurement is purely optical and will not damage the surface of the test subject. In addition, no measurement bias is introduced from any contact force.
- **System self-calibration**
  A self-calibration methodology was developed. The self-calibration enables the metrology system to deduce positions and attitudes of its own sensors without using any additional measuring equipment.

The self-calibration allows excluding errors caused by the assembly inaccuracies and the thermal deformations of the metrology system structure.

- **Sensor combination** (**fusion**) **method** :
  Thanks to an advanced algorithm combining the information from individual sensors, the final accuracy of the system is higher than the accuracy of its components.

Object under Observation

The specific object tracked by the metrology system is the SCM end effector which is called Carrier. It is a small titanium part (40×11×7 mm; 2.4 g) which carries a cartridge with silicon slits. The Carrier moves to change the slit aligned with the sunlight beam. The Carrier is shown in Figure 3. The yellow-marked surfaces are used by the metrology system to track the position and the attitude of the Carrier. Carrier is coated with a black mat coating.

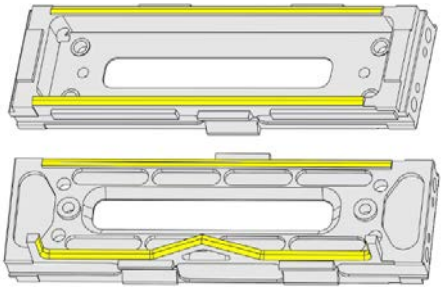

Figure 3. SCM end-effector

Hardware layout

The metrology system hardware is shown in Figure 6, a cut view is shown in Figure 5, and the corresponding diagram is shown in Figure 4. As shown in Figure 4, the whole setup is located in a clean room ⑩. The test subject ⑨ is installed inside of the heat exchanger ⑧. The heat exchanger is a copper structure with observation openings and a channel for the heat transfer fluid. Fluid circulates between the heat exchanger and the external thermostat ⑦. The Heat exchanger is installed inside of the hermetic aluminium chamber ② with sealed glass windows. The chamber is purged through the dedicated valve with high purity nitrogen ⑤ to maintain a low humidity level as well as a cleanliness level better than ISO 5. 2D distance sensors ① are installed on micrometer positioning stages outside the chamber. They observe the test subject through glass windows. Sensor heads and the chamber are supported by the same structure ⑥ which is made of stainless steel and polyvinylidene difluoride (PVDF). Sensor heads are connected to the acquisition devices ③ which, in turn, are connected to the computer ④.

For the particular SCM that is sensitive to microvibration, the system was installed on the optical table with air pneumatic bearings to reduce microvibrations. Mechanical stops protect the test subject and sensors from unintentional contact with other parts of the system during the assembly.

Sensors have a limited operational temperature range, therefore sensor support structures are made of PVDF with multiple holes for a better thermal decoupling from the heat exchanger. The temperature at the interface of the test subject is monitored by thermocouples.

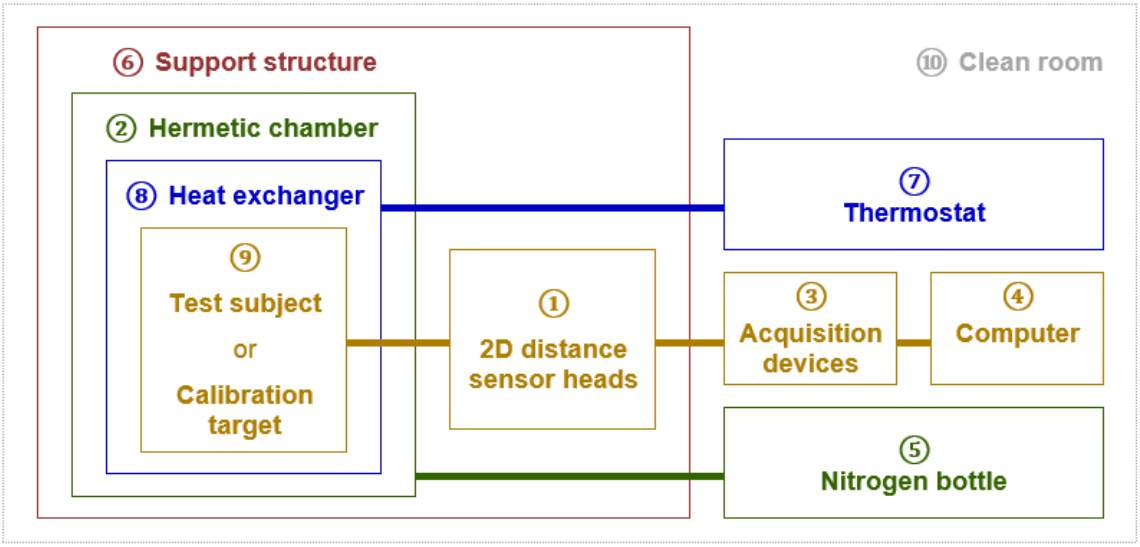

Figure 4. Metrology system diagram

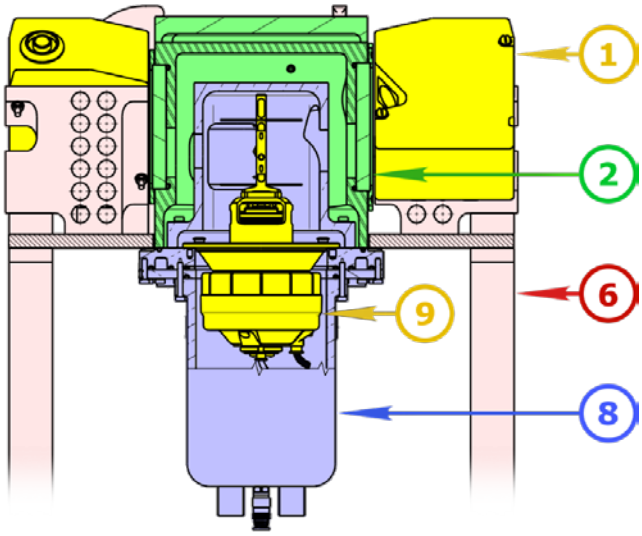

Figure 5. Metrology system cut view

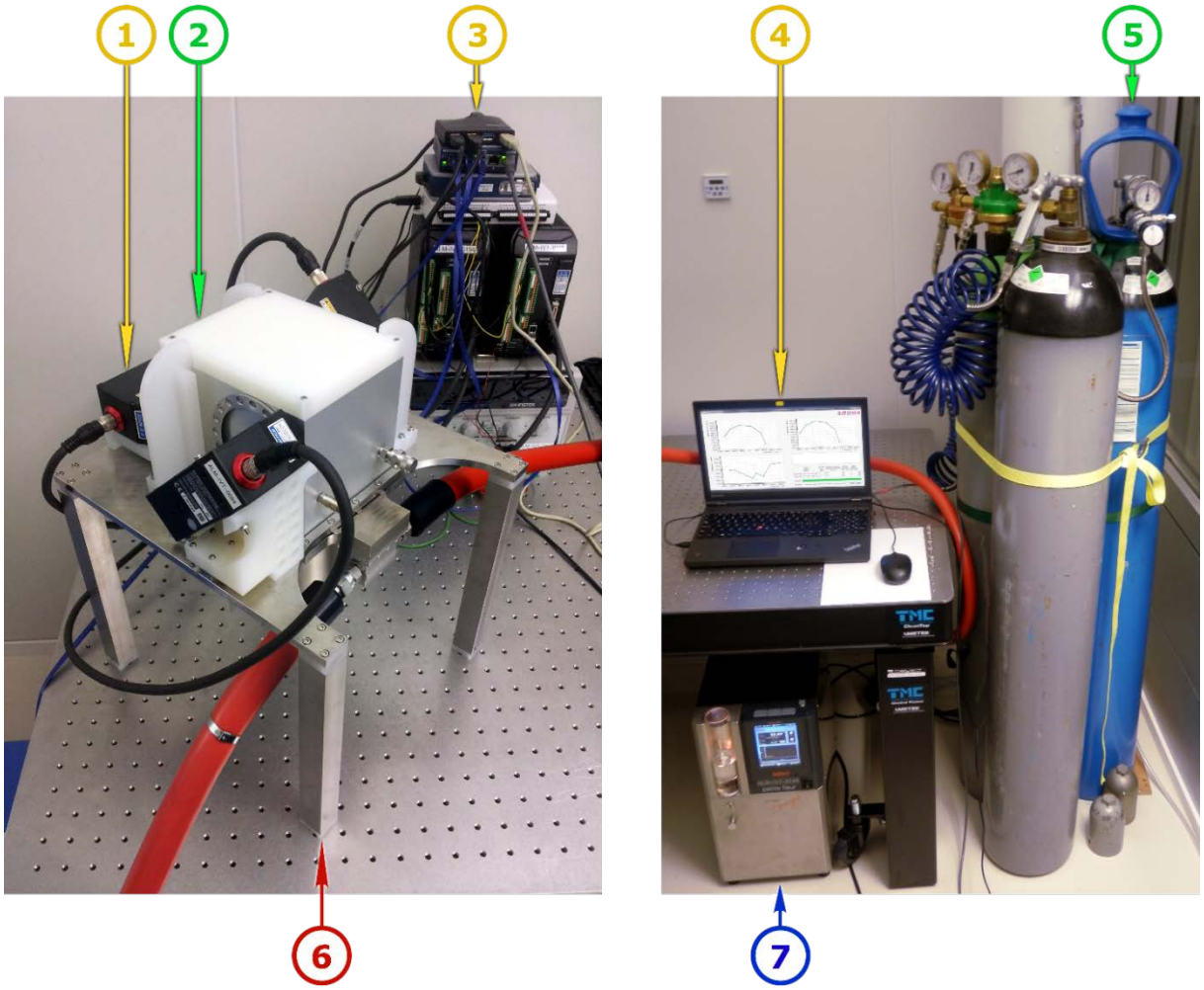

Figure 6. Metrology system hardware

Measuring principle

Specimen position and attitude in 3D are calculated from the raw data acquired by three 2D distance sensors [2] which are aligned as shown in Figure 7. Each 2D distance sensor captures a cross-section of the Carrier as shown in Figure 8. The combination of the 3 cross-sections is processed by a software developed by Almatech to provide an accurate position and attitude.

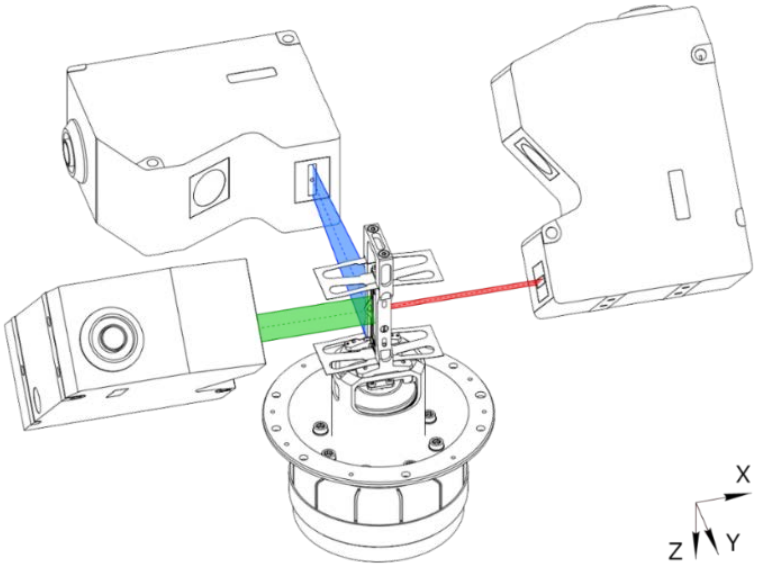

Figure 7. Position and attitude of the sensors

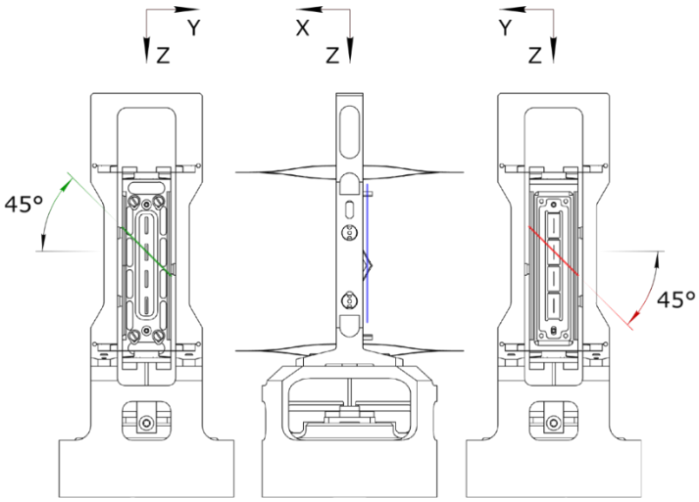

Figure 8. Test subject sections observed by the sensors

The algorithm contains the following major steps:

1. Acquisition of the specimen cross-sections (shown in Figure 8) from the 2D laser distance sensors. Cross-sections are represented by the arrays of points;
2. Fitting the polylines to the acquired points using linear segmented regression. Calculation of polyline vertices coordinates and evaluation and their uncertainties;
3. Calculation of specimen position and attitude by minimizing error between measured vortices and specimen model.

The 1st step (acquisition of raw measured points) is done using application programming interface provided by the sensor manufacturer. Raw measured points are shown in Figure 9 as the blue dots.

In step 2, the software calculates cross-sections vertices coordinates from the measured points coordinates. Cross-section best-fit profile is shown in Figure 9 as a blue polyline. Initial set of points is

split into subsets so that each subset contains points of a single line. The boundaries between subsets are found by minimization of the sum of quadratic mean errors of best-fit lines.

Vertices coordinates are not the only output of the 2nd step. Uncertainty is also automatically estimated for each vertex in order to reach a higher accuracy during sensor fusion. Sensor fusion is a process of combining sensor data such that resulting information has less uncertainty than would be possible when these sources were used individually.

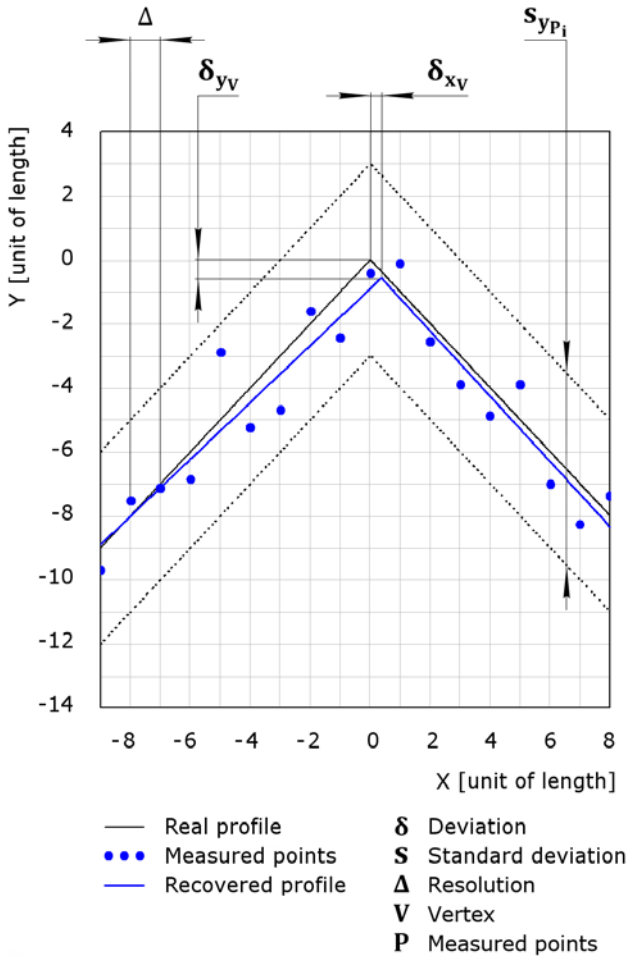

Figure 9. Real and recovered profiles

Uncertainty of each vertex coordinates depends on multiple parameters, such as size and arrangement of lines in the field of view. The equation to estimate the vertices coordinates uncertainty is derived from the following set of equations:

$$y_{L_i}(x) = k_i \cdot x + b_i \tag{1}$$

$$y_{L_1}(x_V) = y_{L_2}(x_V) = y_V \tag{2}$$

$$k_i = \frac{\mathrm{cov}(x_{P_i}, y_{P_i})}{\mathrm{var}(x_{P_i})} \tag{3}$$

$$b_i = \mathrm{mean}(y_{P_i}) - k_L \cdot \mathrm{mean}(x_{P_i}) \tag{4}$$

$$s_{y_{P_i}} = \sqrt{\frac{1}{n_i - 2} \cdot \sum_{j=1}^{n_i} \left(y_{P_{ij}} - y_{L_i}(x_{P_{ij}}) \right)^2} \tag{5}$$

$$x_{P_{ij}} = \left(j - \frac{1}{2} + \Theta \right) \cdot \mathrm{sign}(i) \cdot \Delta \tag{6}$$

$$s_{F(a_1, a_2, \ldots)} = \sqrt{\left(s_{a_1} \cdot \frac{\partial F}{\partial a_1} \right)^2 + \left(s_{a_2} \cdot \frac{\partial F}{\partial a_2} \right)^2 + \cdots} \tag{7}$$

where
- x, y – Coordinates in the sensor frame
- i – Index of the line. The vertex is formed by two lines (1 and 2).
- j – Index of the measured point. Each line may contain deferent number of points.
- $y_{L_i}(x)$ – Best-fit function for the line i.
- k_i – Estimator of the slope coefficient for the line i. It is a trigonometric tangent of the angle between the best-fit line i and the X axis.
- b_i – Estimator of the intercept coefficient for the line i. It characterizes the shift of the best-fit line i along the Y axis.
- x_V, y_V – Coordinates of the vertex which is formed by intersection of two lines.
- cov(…) – Covariance.
- var(…) – Variance.
- mean(…) – Average.
- x_P, y_P – Coordinates of measured points.
- n_i – Quantity of measured points in the line i.
- $s_{y_{P_i}}$ – Estimate of quadratic mean distance (along Y axis) between measured points and the best-fit line i.
- Δ – Resolution of the sensor head. This value is the distance between neighbour measured points along X axis.
- Θ – Coefficient which characterizes the distance between the vertex and the nearest measured points. Its value lays in the range between -0.5 and +0.5.
- $s_{F(a_1, a_2, \ldots)}$ – sample standard uncertainty of some function F with the arguments a_1, a_2, …

Equations 1, 3, and 4 represent a linear regression as per [9]. Regression gives a better result than orthogonal Deming regression due to the specific internal architecture of the sensors. Equation 7 is a well-known variance formula for uncertainty propagation from [10]. Vertex coordinates are derived from equations 1 and 2 as:

$$x_V = \frac{b_2 - b_1}{k_1 - k_2} \quad ; \quad y_V = \frac{k_1 b_2 - k_2 b_1}{k_1 - k_2} \tag{8}$$

Equation 7 is applied to equations 3, 4 and 8 to calculate uncertainties of the vertex coordinates. For that, the coordinate system origin is aligned with the vertex. Coefficient Θ of the equation 6 is assumed equal to 0.5 which is the worst case estimate. The standard uncertainty of the vertex coordinates is:

$$s_{x_V} = 2 \cdot \sqrt{\frac{\left(s_{y_{P_1}}\right)^2}{\eta_1} + \frac{\left(s_{y_{P_2}}\right)^2}{\eta_2}}{(k_1 - k_2)^2} \quad ; \quad s_{y_V} = 2 \cdot \sqrt{\frac{\left(s_{y_{P_1}}\right)^2}{\eta_1} \cdot k_2^2 + \frac{\left(s_{y_{P_2}}\right)^2}{\eta_2} \cdot k_1^2}{(k_1 - k_2)^2} \tag{9}$$

Where η are coefficients which characterize quantity of points in each line as:

$$\eta_1 = \frac{n_i \cdot (n_i - 1)}{n_i + \frac{1}{2}} \tag{10}$$

Once the positions of vertices are calculated, the metrology system software proceeds to the 3rd step which searches for the corresponding position and attitude of the Carrier. This is done by solving the following system of equations. The system is solved using a variation of Nelder–Mead method [11].

$$p^{s^i}_{v_{ijk}} = \boldsymbol{a}^{\,I}_{s_i}{}^{-1} \cdot \left(\boldsymbol{a}^{\,I}_{t} \cdot p^{t}_{v_{ijk}} \cdot \boldsymbol{a}^{\,I}_{t}{}^{-1} + p^{I}_{t} - p^{I}_{s_i} \right) \cdot \boldsymbol{a}^{\,I}_{s_i} \tag{11}$$

Conversion of vertices coordinates from Carrier frame to sensor frame. See Figure 11.

$$p^{s^i}_{e_{ij}} = p^{s^i}_{v_{ij0}} + \left(p^{s^i}_{v_{ij1}} - p^{s^i}_{v_{ij0}} \right) \cdot \frac{p^{s^i}_{v_{ij0}} \cdot z}{(p^{s^i}_{v_{ij0}} - p^{s^i}_{v_{ij1}}) \cdot z} \tag{12}$$

Intersection point of the line (Carrier edge) and the xy-plane (laser beam of the sensor). See Figure 10.

$$\sum_{i=0}^{n_s - 1} \sum_{j=0}^{n^{s^i}_e - 1} \left(M_{e_{ij}} \cdot \left(p^{s^i}_{e_{ij}} - \tilde{p}^{s^i}_{e_{ij}} \right) \right)^2 = f \to 0 \tag{13}$$

Sum of weighted distances between points (measured and assumed) of intersection.

where
- ● – scalar values
- ● – 3D vectors
- ● – 3×3 matrixes
- ● – quaternions
- $p^{s^i}_{v_{ijk}}$ – assumed position of the Carrier vertex ijk in the coordinate system of the sensor i
- $p^{t}_{v_{ijk}}$ – assumed position of the Carrier vertex ijk in the coordinate system of the Carrier
- $\boldsymbol{a}^{\,I}_{s_i}$ – assumed attitude of the sensor i relative to the SCM interface
- $p^{I}_{s_i}$ – assumed position of the sensor i relative to the SCM interface
- $\boldsymbol{a}^{\,I}_{t}$ – assumed attitude of the Carrier relative to the SCM interface
- p^{I}_{t} – assumed position of the Carrier relative to the SCM interface
- $p^{s^i}_{e_{ij}}$ – assumed position of the point of intersection between flat laser beam of the sensor i and the Carrier edge ij which connects vertices ij0 and ij1 in the sensor i coordinate

system

$\tilde{p}^{s^i}_{e_{ij}}$ – measured position of the intersection point ij defined above

z – binomial unit vector $(0;0;1)^T$ of the sensor coordinate system basis

n_s – number of sensors in the metrology system

$n_e^{s^i}$ – number of the Carrier edges observed by the sensor i

$M_{e_{ij}}$ – scale matrix which contains the uncertainty of measured intersection point ij

$$M_{e_{ij}} = \begin{bmatrix} \left(s^x_{e_{ij}}\right)^{-1} & 0 & 0 \\ 0 & \left(s^y_{e_{ij}}\right)^{-1} & 0 \\ 0 & 0 & 0 \end{bmatrix}$$

$s^x_{e_{ij}}$ – uncertainty of X-coordinate of the intersection point ij

$s^y_{e_{ij}}$ – uncertainty of Y-coordinate of the intersection point ij

f – objective function which shall be minimized. It characterizes the deviation of the assumed intersection points from the measured intersection points

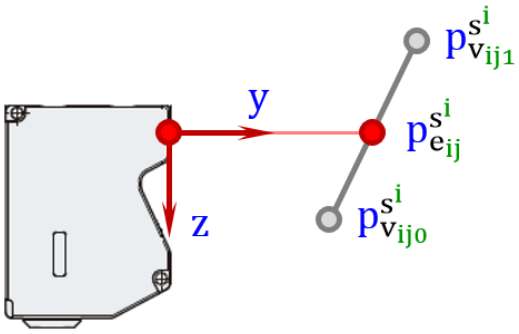

Figure 10. Intersection point of the Carrier edge and the laser beam of the sensor

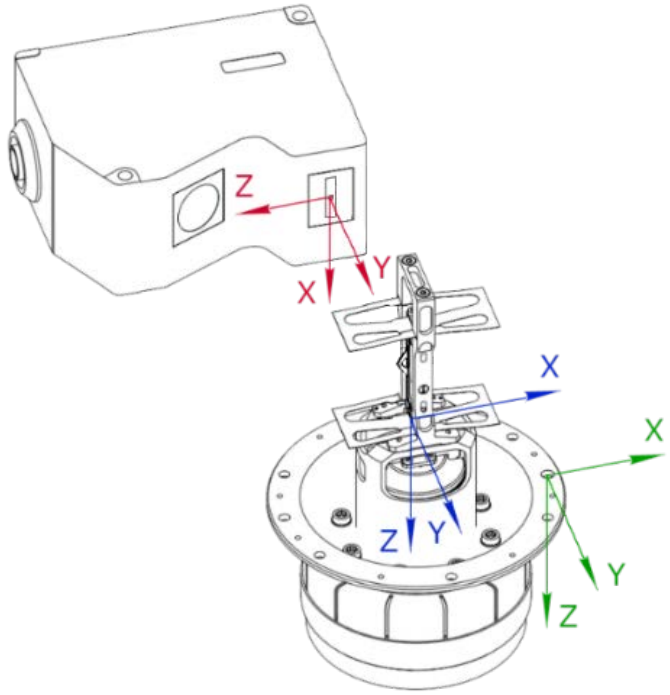

Figure 11. Coordinate systems (frames). Red is a sensor frame. Blue is a Carrier frame. Green is a SCM interface frame.

Self-Calibration

To reach high accurate measurements, both Carrier's geometry and positions of the sensors shall be known. Carrier's geometry is measured before test using the coordinate measurement machine. Positions and attitudes of the sensors are calculated during a so-called self-calibration process. The sensors measure a calibration target (shown in Figure 12) which has known geometry and position in SCM interface frame. The geometry of the calibration target was optimized to determine the position and

attitude of each sensor using a single cross-section which is captured by the same sensor. Cross-sections observed by the three different sensors are shown in Figure 13.

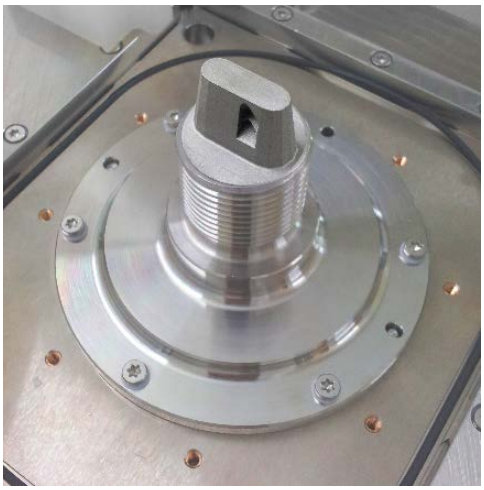

Figure 12. Calibration target

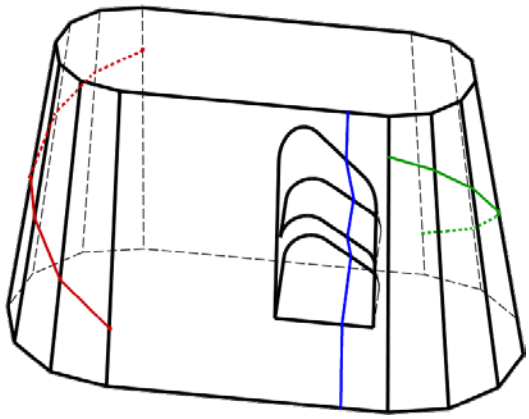

Figure 13. Calibration target sections observed by sensors

The calibration target is made out of Invar to minimize thermal expansion effects. This allows accurate measurement over a specific temperature range.

Position and attitude of each sensor is deduced several times for different temperature points. This approach allows minimizing the errors caused by the thermal deformation of the metrology system structure. Self-calibration also minimizes the bias caused by the deflection in the glass windows. Calibration target sections, as they appear in acquisition software interface written by Almatech, are shown in Figure 14 (refer to Figure 13 for sensor positions).

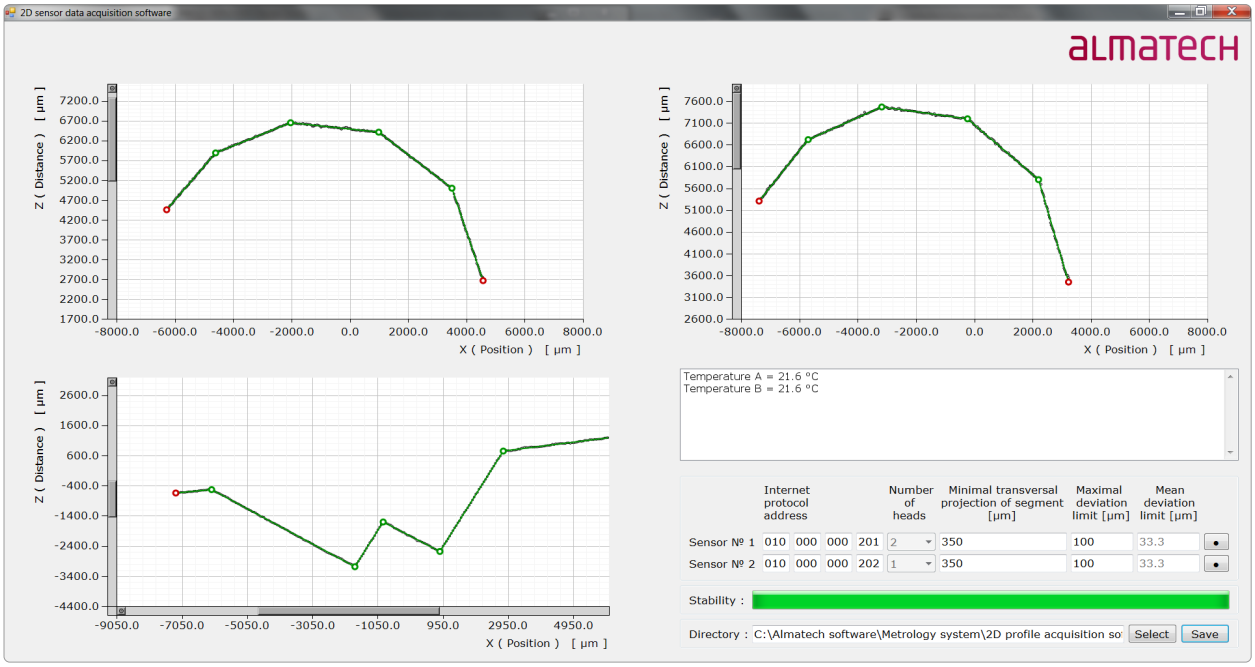

Figure 14. Calibration target sections as they appear in the acquisition software interface

Results

Multiple real-life tests and software simulations were performed to determine the final accuracy of the metrology system with a high level of confidence. The tests were the following:

- Test of self-calibration accuracy (sensors positions self-determination accuracy);
- Test of inaccuracy caused by remounting of test subject and calibration target;
- Test of sensors accuracy with the representative surface optical properties;
- Test of sensors accuracy with the representative geometry.

The estimated result accuracy of the system is shown in Table 1.

Table 1. Measurement uncertainty of the metrology system

Parameter	**Translation** [µm]			**Rotation** [arcsecond]		
	X	**Y**	**Z**	**X**	**Y**	**Z**
Repeatability	0.7	0.4	2.3	11	20	14
Absolute coordinates' accuracy	14.4	23.3	52.4	68	178	570

Lessons learned

For accurate sensor fusion, it is important to take into account that the measurement uncertainty is different for each measurement. Measurement uncertainty of the vertex coordinates depends on multiple parameters, such as size and arrangement of lines in the field of view. The values specified in the sensor datasheet are deduced by the manufacturer for a very particular test case, therefore they cannot be considered as an accurate estimate. For proper evaluation of the vertices coordinates' uncertainty, Almatech derived the equation 9 and performed multiple tests.

It is also important to take into account that the accuracy and reliability of laser distance sensors depends strongly on the optical properties of observed surface. For better and consistent performance, the surface shall be mat (i.e., reflection shall be diffuse). Several surface treatments of nickel-iron alloy were tested (see Figure 16). Micro-ball shot-peening was selected because it showed the best combination of high performance and low impact on specimen's geometry.

From right to left :

1. M : Shot peening + Passivation
2. M+Nc : Shot peening + Chemical nickel plating
3. Nc : Chemical nickel plating
4. Ngm : Mat galvanic nickel plating
5. no label : Passivation only

Figure 15. Surface treatment samples

Outlook

The metrology system will be used at each stage of Slit Change Mechanism test sequence to monitor possible changes of its accuracy. The accuracy checks will be performed after the SCM assembly, the vibration tests, the shock test, the thermal vacuum tests and the life-cycling. All tests which require actuation of SCM will also be performed in the chamber of the metrology system in order to prevent SCM bearings coating from oxidation.

Conclusion

A unique metrology system (hardware and software) for simultaneous precise contactless measurements of 6 degrees-of-freedom of the Solar Orbiter Slit Change Mechanism Carrier is implemented. It features high accuracy, cleanliness, and temperature control. Tests and simulations show that the measurement accuracy of an object absolute position is of 20 micron in in-plane measurement (XY) and about 50 micron out of plane (Z). The typical absolute attitude is determined with an accuracy better than 3 arcmin in rotation around X and Y and better than 10 arcmin in Z. The metrology system is able to determine relative position and movement with an accuracy one order of magnitude lower than the absolute accuracy. Typical relative displacement measurement accuracies are better than 1 micron in X and Y and about 2 micron in Z. Finally, the relative rotation can be measured with accuracy better than 20 arcsec in any direction.

Acknowledgements

To Keyence (Switzerland and Belgium) for support in accessing the available sensors compatible to our surface treatment requirements.

References

1. Paciotti G., Humphries M., Rottmeier F. and Blecha L. "Development and preliminary testing of a high precision long stroke Slit Change Mechanism for the SPICE instrument." *Proceedings of the 42nd Aerospace Mechanisms Symposium, NASA Goddard Space Flight Center*, (May 2014), pp. 31-44.
2. Technical specification of Keyence 2D distance sensors « LJ-V »
   Access : http://www.keyence.com/products/measure/laser-2d/lj-v/specs/index.jsp
   [accessed 2015-09-27]
3. Technical specifications of Handyscan 3D handheld 3D Scanner [Online]
   Access : http://www.creaform3d.com/en/metrology-solutions/products/portable-3d-scanner/technical-specifications-handyscan-3d
   [accessed 2015-08-30]
4. Technical specification of Keyence 3D laser scanning confocal microscope VK-X [Online]
   Access : http://www.keyence.com/products/microscope/laser-microscope/vk-x100_x200/specs/index.jsp
   [accessed 2015-08-30]
5. Description of Lyncée Tec reflection digital holographic microscope [Online]
   Access : http://www.lynceetec.com/reflection-dhm/#1
   [accessed 2015-09-27]
6. Technical specification of Nikon X-ray inspection system MCT225 [Online]
   Access : http://www.nikonmetrology.com/en_EU/Products/X-ray-and-CT-Inspection/Metrology-CT/MCT225-for-Metrology-CT-Absolute-accuracy-for-inside-geometry/(specifications)
   [accessed 2015-08-30]
7. Description of Huber temperature control system « Petite Fleur » [Online]
   Access : http://www.huber-online.com/en/product_listing.aspx?group=1.01
   [accessed 2016-01-20]
8. Description of Acktar coating « Fractal Black » [Online]
   Access : http://www.acktar.com/category/FractalBlack
   [accessed 2016-01-20]
9. Kenney J.F. and Keeping E.S. "Linear Regression and Correlation." *Ch. 15 in Mathematics of Statistics, Pt. 1, 3rd edition,* Princeton, New Jersey, (1962), pp. 252–285.
10. Ku H. H. *"Notes on the use of propagation of error formulas"*. *Journal of Research of the National Bureau of Standards, Vol. 70C, No 4,* (October 1966), pp. 263-273.
11. Nelder J.A., Mead R. "A simplex method for function minimization." *Computer Journal 7*, (1965), pp. 308–313.